APPLIED SCIENCES AND ENGINEERING

Protecting ice from melting under sunlight via radiative cooling

Jinlei Li[1]†, Yuan Liang[2]†, Wei Li[3]†, Ning Xu[1]†, Bin Zhu[1], Zhen Wu[1], Xueyang Wang[1], Shanhui Fan[4], Minghuai Wang[2]*, Jia Zhu[1,5]*

As ice plays a critical role in various aspects of life, from food preservation to ice sports and ecosystem, it is desirable to protect ice from melting, especially under sunlight. The fundamental reason for ice melt under sunlight is related to the imbalanced energy flows of the incoming sunlight and outgoing thermal radiation. Therefore, radiative cooling, which can balance the energy flows without energy consumption, offers a sustainable approach for ice protection. Here, we demonstrate that a hierarchically designed radiative cooling film based on abundant and eco-friendly cellulose acetate molecules versatilely provides effective and passive protection to various forms/scales of ice under sunlight. This work provides inspiration for developing an effective, scalable, and sustainable route for preserving ice and other critical elements of ecosystems.

INTRODUCTION

Protecting ice from melting under sunlight in a sustainable way is highly desirable as it entwines several crucial aspects of our lives: from daily ice/iced food to ice sports and iceberg at high altitudes/latitudes (*1*, *2*). It is estimated that the cold chain alone, required for preserving 40% of the world's food (~400 million tons), is consuming 11% of the global electricity and leading to approximately 2.5% of the world's greenhouse gas emissions (*3*–*5*). As the first step, it is essential to examine the energy flows of the ice systems under sunlight. The representative thermal flows of ice at different latitudes are summarized in Fig. 1A (text S1 and fig. S1) and Fig. 1B. The diagrams reveal that solar radiation (0.3 to 2.5 μm) is the dominating thermal load, leading to an increase in ice temperature and consequential melt. Meanwhile, mid-infrared radiation (2.5 to 18 μm) is the primary energy stream to offset this trend. Therefore, it is clear that imbalanced energy flow is directly relevant to ice melt under sunlight, and it is of great practical significance to explore a sustainable pathway to balance them, therefore enabling passive preservation of various ice systems under sunlight.

Recently, the burgeoning developments in daytime radiative cooling offer a promising strategy to balance the energy flows (*6*–*16*). In these pioneering works, various intriguing materials and structures were developed, such as multilayer/patterned photonic structures (*17*–*19*), nanoparticle-based/porous polymer film (*20*–*23*), cooling wood (*24*), and super-white paints (with solar reflectivity larger than 0.95) (*21*, *25*). Typically, an experimental cooling power of 40 to 100 W m^{-2} and a subambient cooling temperature of 3° to 13°C are demonstrated during a sunny day.

However, for the purpose of preserving ice under sunlight, there are several stringent requirements beyond traditional considerations. First, ice has a much lower temperature compared with most reported scenarios, and therefore, it demands very high radiative cooling performance. For example, it is calculated that an increase of net radiation power from 70 to 110 W m^{-2} can prevent ice/iced food from melting without additional refrigerated devices (fig. S2 and detailed in text S2). In addition, for the specific purpose of ice preservation, it is critical that the radiative cooling materials have to be extremely abundant and scalable (~million metric tons) with minimized environmental impact (*26*–*28*).

In this work, we demonstrate a hierarchically designed film based on abundant and eco-friendly cellulose acetate (CA). This hierarchical CA film is carefully tailored for achieving high cooling performance. The intrinsic vibrations of the molecular bonding endow the CA film with broadband and high mid-infrared emissivity (Fig. 1C), which is desirable for high-performing large-scale cooling, as explained in the model later. Tailored pores act as effective scattering centers for incoming solar radiation (Fig. 1D). Therefore, the hierarchically designed CA film is able to minimize the thermal load on ice under sunlight and realize effective passive protection for ice systems at different latitudes. CA is chosen to construct the film as it is eco-friendly and abundant. CA is biodegradable and can be digested by microorganisms in nature (Fig. 1E) (*29*–*31*). Raw CA is derived from natural cellulose that exists extensively within plant cytoderm (Fig. 1F) (*32*, *33*).

RESULTS

Design, fabrication, and characterizations of the CA film

Broadband and effective reflection of sunlight is essential for realizing radiative cooling under sunlight. Our theoretical models (Fig. 2A and detailed in text S3) reveal that for the CA-based film, a porous structure with multiscale pores ranging from 500 nm to 3 μm supports strong scattering and reflection of sunlight (wavelength range: 300 nm to 2.5 μm). Therefore, we developed a CA molecule–based scalable film (Fig. 2B) via the roll-to-roll electrospinning technique (fig. S3). Its microscopic picture is presented in Fig. 2C. It shows

[1]National Laboratory of Solid State Microstructures, College of Engineering and Applied Sciences, Jiangsu Key Laboratory of Artificial Functional Materials, Collaborative Innovation Center of Advanced Microstructures, Nanjing University, Nanjing 210023, P. R. China. [2]Joint International Research Laboratory of Atmospheric and Earth System Sciences, School of Atmospheric Sciences, Nanjing University, Nanjing 210023, P. R. China. [3]GPL Photonics Lab, State Key Laboratory of Applied Optics, Changchun Institute of Optics, Fine Mechanics and Physics, Chinese Academy of Sciences, Changchun 130033, P. R. China. [4]Department of Electrical Engineering, Ginzton Laboratory, Stanford University, Stanford, CA 94305, USA. [5]Frontiers Science Center for Critical Earth Material Cycling, Nanjing University, Nanjing 210023, P. R. China.
*Corresponding author. Email: jiazhu@nju.edu.cn (J.Z.); minghuai.wang@nju.edu.cn (M.W.)
†These authors contributed equally to this work.

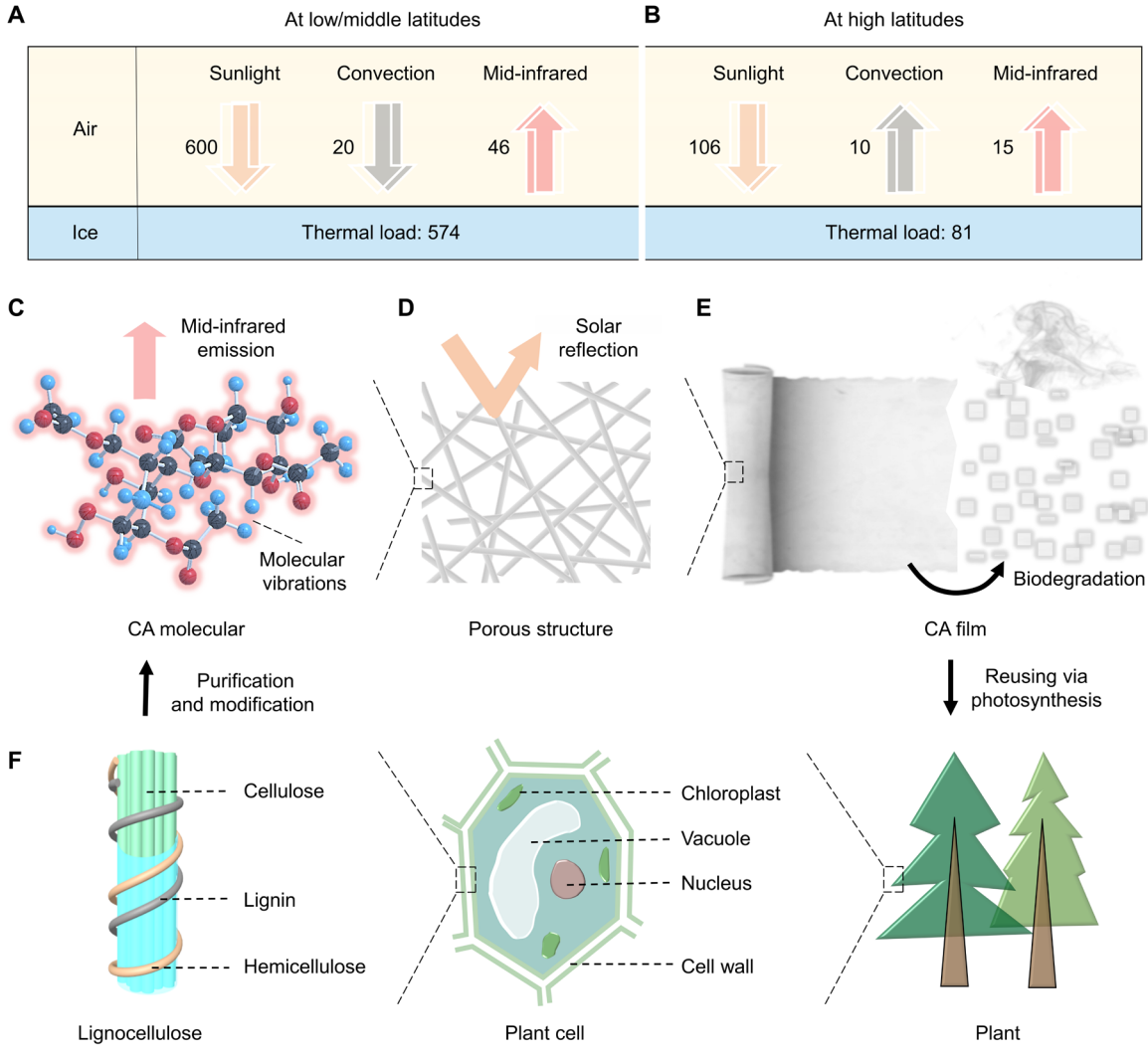

Fig. 1. Hierarchically designed and eco-friendly CA film for passive protection of ice under sunlight via radiative cooling. Energy transfer process of ice systems at (**A**) low/middle and (**B**) high (>70.5°N) latitudes, respectively, in a unit of watts per square meter. The solar irradiation and mid-infrared emission are the dominant energy input and output for both scenarios. The unbalanced energy flows lead to the melt of ice. (**C** to **F**) Hierarchical designs and life cycle of the porous CA film for realizing passive ice protection via radiative cooling. (C) The intrinsic molecular vibrations and (D) porous structure endow the CA film with high mid-infrared emissivity and solar reflectivity, respectively. Therefore, the thermal loads on the ice systems are substantially reduced with the hierarchically designed film. (E) At the end of the life cycle, the hierarchically designed CA film can be decomposed by the natural microorganism to reproduce CA (right). (F) The abundant raw materials of the hierarchically designed CA film can be derived from the cytoderm of natural plants.

that nanofibers connect and form multiple pores with sizes in the same range as the theoretical design (fig. S4), ideal for scattering sunlight. The reflectivity spectrum of the hierarchically designed CA film in Fig. 2D (left, before the break) confirms that weighted reflectivity is as high as 0.974 for the solar spectrum (AM 1.5G).

High mid-infrared emissivity is critical to send heat flow to the cold universe (3 K) to realize radiative cooling. Organic macromolecules offer a convenient knob for tailoring the mid-infrared emission, as every molecular bonding corresponds to specific mid-infrared vibration wavelengths (*34*–*36*). Besides, deformation, together with the amorphousness of macromolecular chains, is beneficial to broaden and enhance these vibrations (*37*, *38*). For the CA film, the multiple bonding of C—O and C—O—C of CA molecules (fig. S5) provides a strong mid-infrared emission at the atmospheric transparent window (8 to 13 μm). In addition, the relevant bonding of OH, C═O, and CH_2 contributes to high emissivity across the rest of the mid-infrared bands. As our expectations, the mid-infrared emissive spectrum in Fig. 2D (right, after the break) verifies that the hierarchically designed CA film has a broadband mid-infrared emissivity of 0.92 with an emissive peak at the atmospheric transparent window. This broadband mid-infrared emissivity is ideal for cooling large-scale ice at high altitudes, as explained in the modeling experiment later.

With the desired optical properties for CA film achieved via hierarchical designs, we next measured the cooling temperature and cooling power of the hierarchically designed CA film to evaluate its radiative cooling performances. Here, the cooling temperature is defined as the temperature reduction of the film from the ambient temperature. A cooling power of up to ~110 W m^{-2} and a cooling temperature of ~12°C are realized by the hierarchically designed CA film under direct sunlight irradiation (Fig. 2E; theoretical estimation

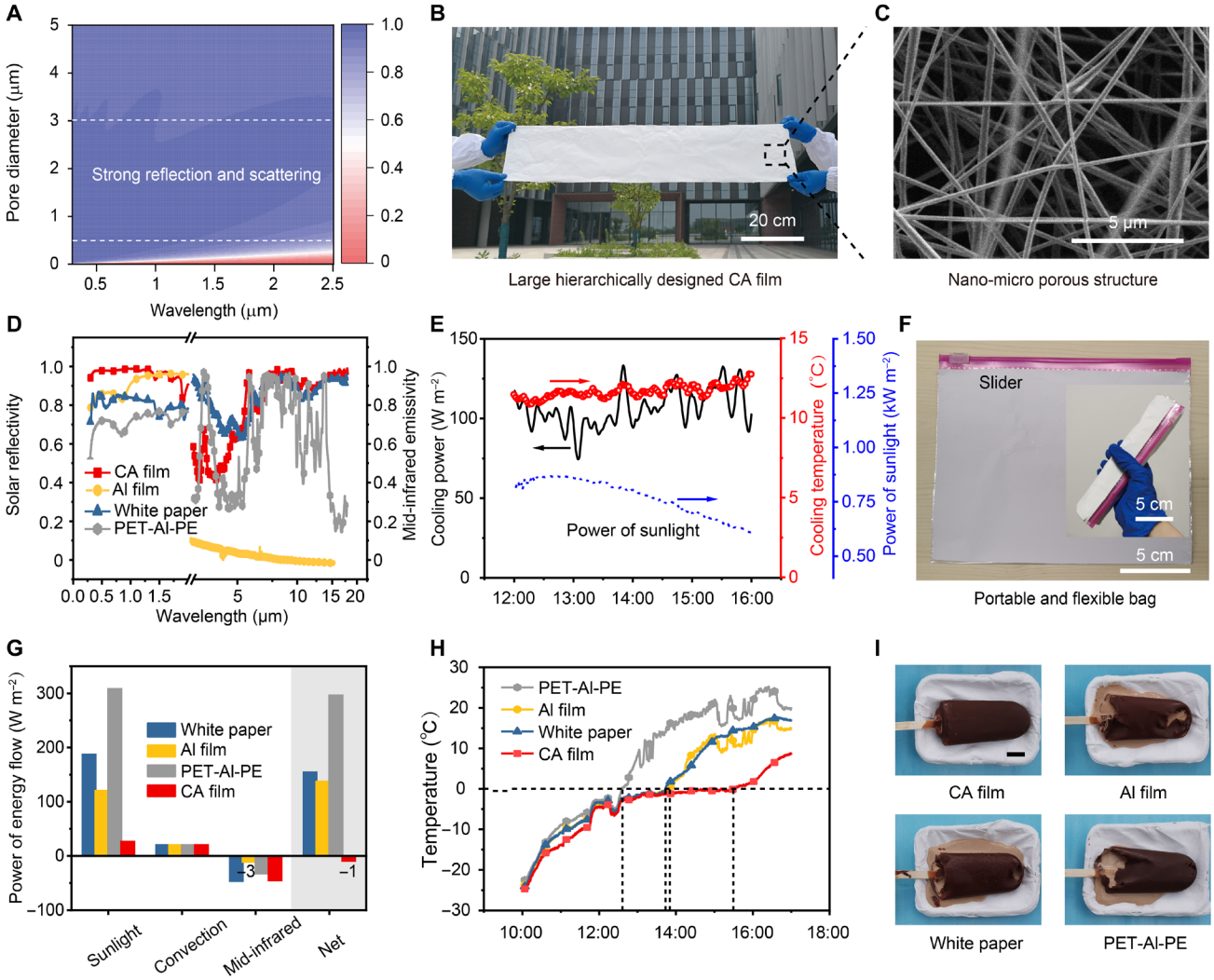

Fig. 2. Outdoor ice/iced-food preservation at low/middle latitudes. (**A**) Theoretical analysis of the pore's scattering effect on the incident sunlight. The color bar represents reflectivity. (**B**) A photograph of the hierarchically designed CA film. (**C**) An SEM image of the hierarchically designed CA film. (**D**) Solar reflectivity (left axis, before the break) and mid-infrared emissivity (right axis, after the break) spectra of the hierarchically designed CA film. The spectra of white paper, Al film, and PET-Al-PE film are shown for comparison. (**E**) Cooling performance under sunlight referring to the ambient of the hierarchically designed CA film. (**F**) A photograph shows that the hierarchically designed CA film is tailored into a homemade portable and flexible bag specifically for outdoor ice/iced-food preservation. The pink bar is a slider. (**G**) Energy flows of ice/iced food wrapped by different packing materials. (**H**) The temperature evolutions (left axis) of the iced food with different packing ways under sunlight. (**I**) Photographs of the ice creams after ~80 min of sunlight exposure (~540 W m^{-2}). Scale bar, 2 cm. The hierarchically designed CA film provides the best preservation. Photo credit of (B), (F), and (I): Jinlei Li and Ning Xu, Nanjing University.

is provided in text S4 and figs. S6 and S7), confirming the excellent radiative cooling capacity of the hierarchically designed CA film.

Ice/iced-food preservation

The hierarchically designed CA film with such excellent radiative cooling performances can be conveniently tailored to various forms, such as a portable and flexible bag specifically for outdoor ice/iced-food preservation (Fig. 2F). The three most commonly used packing materials, including white paper, aluminum (Al) film, and polyethylene terephthalate (PET)–Al–polyethylene (PE) film, are used as controls. In contrast to the hierarchically designed CA film, white paper, Al film, and PET-Al-PE film have much lower solar reflectivity of only 0.806, 0.880 (the highest one in many commercialized products we bought; fig. S8), and 0.692, respectively (Fig. 2D, left axis). Besides, all of them have lower mid-infrared emissivity than the hierarchically designed CA film: 0.89 for white paper, 0.05 for Al film, and 0.62 for PET-Al-PE film, respectively (Fig. 2D, right axis). On the basis of their optical properties, we evaluate the thermal load on outdoor ice/iced food (at low/middle latitudes) with these packings and show the results in Fig. 2G (see text S5 and fig. S9 for a detailed analysis). It is found that the thermal loads on the ice/iced food with white paper, Al film, and PET-Al-PE film are as high as 154, 137, and 296 W m^{-2}, respectively, leading to the consequent rapid melt of outdoor ice/iced food. In contrast, the hierarchically designed CA film substantially reduces the thermal load on the outdoor ice/iced food to −1 W m^{-2}, showing its potential in preserving ice/iced food under sunlight.

The changes in thermal load lead to different temperatures of outdoor ice/iced food. We monitored the temperature evolutions of

iced food wrapped by different materials under natural outdoor sunlight irradiation (fig. S10). The results in Fig. 2H show that the duration for the iced food covered with the hierarchically designed CA film to stay below 0°C is about 5.5 hours (the outdoor conditions of sunlight illumination and ambient temperature in fig. S11). In contrast, the durations for iced food to stay below 0°C when wrapped with white paper, Al film, and PET-Al-PE film are 3.7, 3.8, and 2.6 hours, respectively. Our comparative experiments in fig. S12 also confirm that the different melting process of ice/iced food is dominated by the optical properties of packing materials (or above thermal load) rather than the thermal resistance arising from poor contact between ice/iced food and the hierarchically designed CA film.

The prolonged duration below 0°C not only can save a notable amount of energy for cooling but also is beneficial for preserving outdoor ice/iced food. For example, we put commercialized ice creams into portable bags made from the hierarchically designed CA film, white paper, Al film, and PET-Al-PE film and exposed them under outdoor sunlight (fig. S13). It is found that the hierarchically designed CA film provides the most effective passive preservation for ice cream (Fig. 2I), with ~98% integrity after 80 min of sunlight exposure (~540 W m^{-2}). By contrast, approximately less than 50% of ice creams stay unmelted in the white paper, Al, and PET-Al-PE bags. We also make comparisons between the hierarchically designed CA film and the commercially available cooling solutions including polished Al, Al foam (two kinds), and white paint (detailed in figs. S14 and S15). The hierarchically designed CA film consistently shows the best cooling performance and therefore provides the most effective protection for ice under sunlight.

Protection for ice and snow

Balancing the solar input and mid-infrared output is not only crucial for outdoor ice/iced-food preservation but is also the dominant factor for maintaining the ecosystem at high latitudes. Here, ice and snow surface (tiny ice crystals) are two representative geomorphologies. They have different solar reflectivity but similar mid-infrared emissivity (*39*–*41*). In the following, we will demonstrate the passive cooling effects of the hierarchically designed CA film for both ice and snow surfaces.

As indicated in Fig. 1B, the melt of ice at high latitudes is dominated by radiative energy transfer processes of the incident solar radiation and mid-infrared radiative output. As both the incident solar radiation and mid-infrared radiative output are independent of the scale of surface area, we can start via small-scale experiments to evaluate the cooling effects of the hierarchically designed CA film on ice at high latitudes (*42*). A custom-made device, as shown in Fig. 3A and fig. S16, was developed to simulate an ambient temperature at high latitudes [0° to 8°C in years from 2000 to 2100 (*43*)]. From Fig. 3B, it is obvious that the hierarchically designed CA film lowers the temperature of ice. A temperature difference of up to 6.3°C is observed between those with and without the hierarchically designed CA film. As shown in Fig. 3C, even under a mean solar irradiation of ~700 W m^{-2},

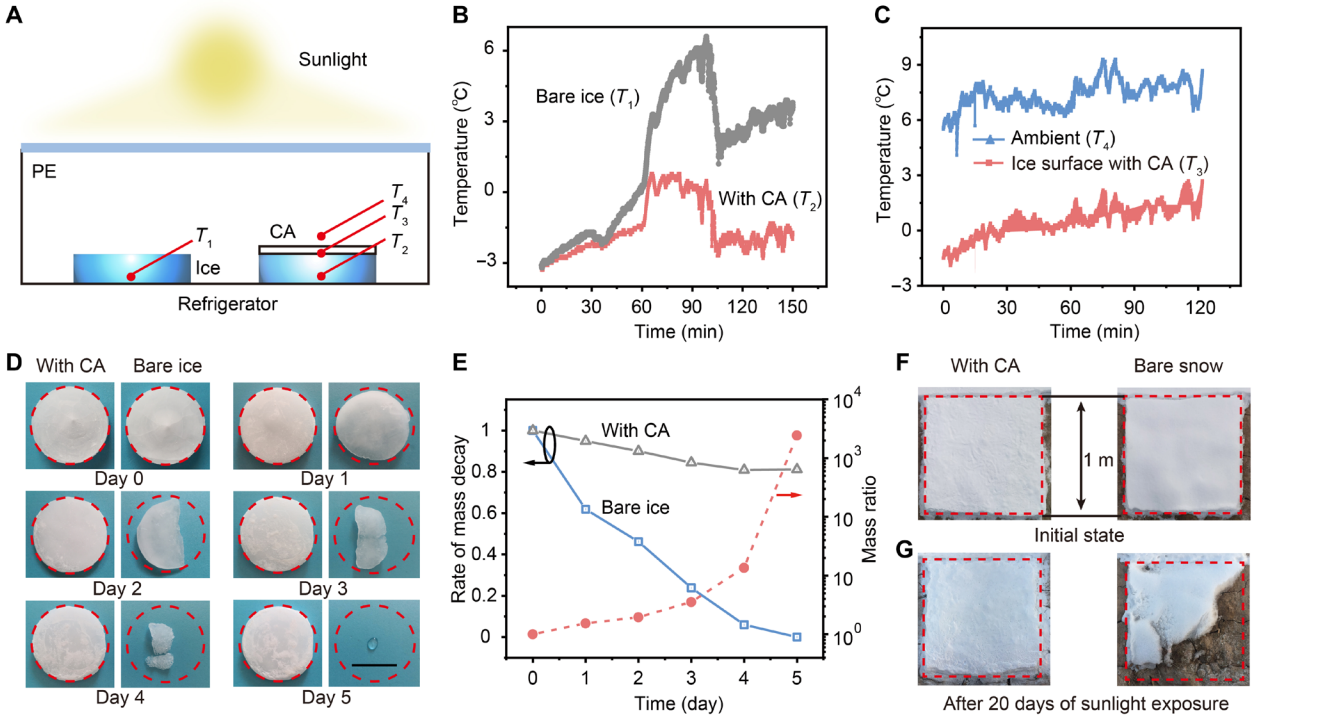

Fig. 3. Ice and snow protection via the hierarchically designed CA film. (**A**) A schematic of the custom-made device for verifying the cooling effects of the hierarchically designed CA film for ice. A refrigerator is used to simulate the atmosphere temperature at high latitudes under sunlight. (**B**) Comparison of the temperature of ice between with and without the hierarchically designed CA film. (**C**) Subambient cooling enabled by the hierarchically designed film under intense illumination of sunlight of ~700 W m^{-2} (higher than the case at high latitudes of below 350 W m^{-2}). (**D**) Photographs show the mass evolution of ice with (left) and without (right) the hierarchically designed CA film. Scale bar (in black), 2 cm. (**E**) Mass decay of the ice with and without the hierarchically designed film (left axis). The mass ratio of the unmelted ice is also shown (right axis). (**F** and **G**) Protection for snow. Photographs show snow (F) at the initial state and (G) after 20 days of outdoor sunlight exposure. Snow melt is slowed thanks to the protection of the hierarchically designed CA materials. Photo credit of (D), (F), and (G): Jinlei Li and Ning Xu, Nanjing University.

which is much stronger than the case at high latitudes [below 350 W m^{-2} (*44*)], the surface temperatures of ice with the hierarchically designed CA film stay ~7°C lower than that of ambient.

The lowered ice temperature is very beneficial for slowing ice melt. To verify the effect of preservation, we exposed the identical pieces of ice with and without the hierarchically designed CA film (in the custom-made device) under natural sunlight (fig. S17) for five successive days (from 6:00 a.m. to 12:30 a.m. every day). Their mass evolutions were recorded and shown in Fig. 3D. It is clear that the size of ice with the hierarchically designed CA film remains unchanged. In contrast, the bare ice shrinks and disappears. The mass decay curves in Fig. 3E are well corresponding to the tendency shown by photographs. These results confirm that the hierarchically designed CA film provides effective protection for ice under sunlight.

Besides ice, the hierarchically designed CA film also shows excellent protection for snow surface, another typical geomorphology at high latitudes. We carried out field testing for snow surfaces with and without the hierarchically designed CA. Initially, the two pieces of snow were intentionally controlled to have nearly identical shapes and mass (Fig. 3F and fig. S18). After 20 days of outdoor sunlight exposure (fig. S19), the remains of snow with the hierarchically designed CA materials are found to be ~50% more than that of the bare snow (Fig. 3G and fig. S20). Furthermore, we performed ~80 m^2 of outdoor test (without a PE cover) in Tianshan Glacier No. 1 (Xinjiang, China; see more details in fig. S21). Previously, geotextile, a common material, has been used for covering the glacier (*45*, *46*). It is found that, after 20 days, the glacier covered by a radiative cooling film is ~0.7 m higher than that without any cover. These results provide direct proof that our radiative cooling film is effective in slowing the melt of local glaciers.

Modeling the cooling effects for ice at high latitudes

Via the above small-scale experiments, it is clear that the hierarchically designed film provides effective cooling for both ice and snow. To predict the scale-up implication, we use modeling to evaluate the cooling impacts. In Fig. 4A, an iceberg (chunks of ice breaking off from parent glaciers) with a size of dozens of square kilometers (equivalent to the size of a large ski resort) is first studied via a thermodynamic model (see text S6 for details). It is found that the iceberg lost 1 m through melt during the summer season. In contrast, the hierarchically designed CA film enables a 1-m thickening of the iceberg. Furthermore, we use climate model experiments to extend the hierarchically designed CA film onto sea ice within the Beaufort Gyre region, the annulus between 70.5°N and 80.5°N and the north of 70.5°N (text S7). The 5 to 40% increase of concentration (Fig. 4, B to D) and 0.5- to 2.5-m thickening (fig. S22) of sea ice from with and without the CA film within these specified areas show that our approach is capable of effective regional/targeted protection for the ice systems at high latitudes.

Such exciting preservative potential of the hierarchically designed CA film is attributed to its excellent radiative cooling capacity due to both high solar reflectivity and mid-infrared emissivity across broadbands. As shown in Fig. 4E, the hierarchically designed CA film leads to a distinct enhancement in the solar reflectivity (above 0.20) at high latitude. We summarize the main energy fluxes of the high latitudes with and without the hierarchically designed CA film in Table 1. It reveals that the enhanced solar reflectivity plays a primary role in lowering the surface thermal load. Meanwhile, the output energy in the forms of mid-infrared radiation and convection is nearly unaffected. Consequently, the surface temperature at high latitudes decreases by around 4°C (Fig. 4F).

Note that for large-scale application at high latitudes, the broadband and high mid-infrared emissivity, as illustrated by the hierarchically

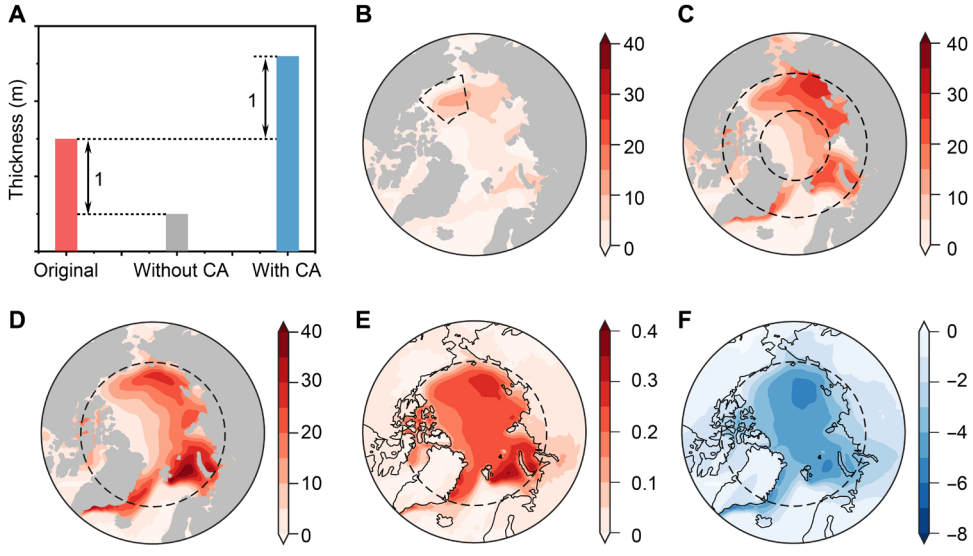

Fig. 4. Ice protection at high latitudes. (**A**) Thickness change of an iceberg (with a size of dozens of square kilometers). The hierarchically designed CA film can effectively protect an iceberg from melting during the summer season. (**B** to **D**) Maps show the differences of sea ice concentration (in the unit of %) between with and without the hierarchically designed CA film. The CA film is applied over the sea ice within (B) the Beaufort Gyre region, (C) the annulus between 70.5°N and 80.5°N, and (D) the north of 70.5°N, respectively. These applied areas are labeled by dark dashed lines. The hierarchically designed CA film is capable of effectively regional/targeted protection for the ice at high latitudes. (**E** and **F**) Maps of the differences in surface (E) solar reflectivity and (F) temperature (unit in kelvin) between with and without the hierarchically designed CA film, respectively. The great protective potential for ice at high latitudes of the hierarchically designed CA film is attributed to its excellent sunlight reflection and consequential cooling.

Table 1. Averaged energy fluxes of the high-latitude surface (>70.5°N) under sunlight. The arrows denote the directions of energy transfer referring to the ground: ↓downward and ↑upward; unit, watts per square meter.

	Sunlight ↓	Mid-infrared ↑	Convection ↑	Net ↓
With CA film	66.8	14.9	7.8	44.1
Without CA film	106.2	15.2	10.3	80.7
Difference	−39.4	−0.3	−2.5	−36.6

designed CA film (Fig. 2D), is preferred over the selective emissivity only high at the atmospheric window (selective thermal emitter). This is different from the previous recognition (*6*, *17*, *47*) that the selective thermal emitter is superior for cooling in most other scenarios typically at small scale. For small-scale applications, the temperature of the thermal emitter is typically lower than the ambient temperature, which can only be achieved through combining high-performing radiative cooling with minimized parasitic cooling loss via convection and conduction. However, for large-scale applications of ice protection, it is not practical to prevent the parasitic cooling loss; therefore, it is extremely challenging to maintain the strong positive temperature gradient between the atmosphere and the surface (temperature inversion). The strong near-surface temperature inversion is hardly observed at high latitudes (*48*). For a typical vertical temperature profile, our radiative-convective column model shows that the selective thermal emitter is less effective for cooling and results in more than 6°C temperature increase at the surface compared to a broadband thermal emitter (fig. S23 and see text S8 and table S1 for details). Therefore, for radiative cooling at large scale, broadband thermal emissivity is more desirable, compared to selective thermal emissivity only at the atmospheric window.

Biodegradability at the end of life of the hierarchically designed CA film is another crucial issue that should be given full consideration, no matter for preserving ice/iced food or protecting the ice at high latitudes. Our soil exposure tests (in Nanjing of 31°N) show that the hierarchically designed CA film exhibits the best biodegradability among various polymers for developing radiative cooling materials (fig. S24). Therefore, it offers an environmental-friendly protection for the ice and snow at various latitudes.

DISCUSSION

In summary, we demonstrate that a hierarchically designed CA film provides effective, eco-friendly, and scalable radiative cooling for protecting ice under sunlight. Because of the critical role that ice plays in daily life and ecosystem, it also calls for more persistent and collective efforts to develop a sustainable pathway for ice protection and preservation.

MATERIALS AND METHODS

Fabrication of the hierarchically designed CA film

The hierarchically designed CA film was fabricated via scalable roll-to-roll electrospinning with multineedles (fig. S3). CA (17 weight %) was dissolved in acetone/*N*,*N*′-dimethylformamide [optimized to 4:1 (v/v)] to form a clear solution. A 30-ml syringe equipped with a 20-gauge needle was used for injecting the as-prepared solution with a flow rate of 4 ml hour^{-1}. The voltage difference and tip-to-collector distance were 15 kV and 15 cm, respectively. A drum wrapped with a layer of Al film was used for collecting the CA nanofibers. All electrospinning experiments were carried out at a room temperature of ~20°C and a relative humidity of ~45%.

Material characterizations

The solar reflectivity spectrum was measured by an ultraviolet-visible (UV-vis) near-infrared spectroscope [UV-3600 (SHIMADZU) and LAMBDA 1050+ (PerkinElmer) for double-checking/calibration] equipped with an integrating sphere (ISR-310 and LAMBDA 150-mm InGaAs, respectively). Barium sulfate was used as a reference. A Fourier transform infrared (FTIR) spectrophotometer (Nicolet iS50R, Thermo Fisher Scientific) was used to measure the mid-infrared emissivity spectrum of the Al film. An integrating sphere (4P-GPS-020-SL, Pike) was attached to the FTIR spectrophotometer to measure the emissivity spectrum of other samples if not specified. A gold mirror was used as a reference. The microscopic picture was captured by scanning electron microscopy (SEM; MIRA3, TESCAN). The porosity of the hierarchically designed CA film was measured by mercury intrusion porosimetry (AutoPore Iv 9510, MICROMERITICS).

Measurement of the cooling performance of the hierarchically designed CA film

The cooling temperature of the hierarchically designed CA film was measured via the device shown in the fig. S25. The cooling power was measured via the device, as presented in fig. S26, with a temperature feedback circuit. The temperature of the hierarchically designed CA film was controlled to be equal to the ambient temperature via a heating film. The heating power of this film was used to compensate for the cooling power of the hierarchically designed CA film. Therefore, the cooling power equals to the heating power. This method is consistent with previous studies (*21*, *22*, *24*). The heating power of the film was monitored and recorded by a power meter (66205, Chroma). The cooling temperature and power of the hierarchically designed CA film are shown in Fig. 2E. The incident sunlight power during the measurement is recorded and presented as well.

Outdoor iced-food experiments

The temperatures of the outdoor iced-food wrapped by different packing materials were measured with the devices shown in fig. S10. The optical properties of every case mainly depend on ice cream itself and the top-covering materials, as sunlight or mid-infrared light hardly passes ice creams (fig. S27). The foam as a thermal insulation layer and the sunlight reflector [polyvinylidene difluoride film (solar reflectivity of >0.95), Al reflector (solar reflectivity of >0.95), and Al film (solar reflectivity of ~0.88)] were used to minimize the impacts from the environment. This setup is widely adopted by previous works (*17*, *21*, *24*). The temperatures were real-time measured by thermocouples. To compare the protective effects of different packing materials for the iced food, identical ice creams were enclosed in the custom-made portable bags made from different packing materials. They, together with a bare one without any packing, were exposed under sunlight with a mean power of ~540 W m^{-2} for ~80 min.

Small-scale experiments of ice protection

The comparative experiments to demonstrate the protective effect of the hierarchically designed CA film for ice were carried out via the device shown in fig. S16. The refrigerator with a temperature feedback circuit was used to control the ambient temperature close to the projected surface air temperature at high latitudes [0° to 8°C (*43*)]. We exposed a piece of bare ice and one with the hierarchically designed CA film under natural sunlight and the ambient temperature of 0° to 8°C. The incident sunlight flux is shown in fig. S17. The temperatures of the ice and ambient were measured by thermocouples. The locations of the thermocouples are schematically shown in Fig. 3A.

Field testing of snow protection

Two pieces of identical snow with a size of 1 m by 1 m in the wild of Bayannur, Inner Mongolia, China were used in this experiment. We covered the surface of one piece with the hierarchically designed CA powder and left a bare one for comparison. For outdoor applications, powder is even more convenient. Therefore, hierarchically designed powder is used. The two pieces of snow were exposed to the natural environment for 20 continuous days. The power of incident sunlight is shown in fig. S19.

SUPPLEMENTARY MATERIALS

Supplementary material for this article is available at https://science.org/doi/10.1126/sciadv.abj9756

REFERENCES AND NOTES

1. A. Witze, Dramatic sea-ice melt caps tough Arctic summer. *Nature* **573**, 320–321 (2019).
2. R. E. Bell, H. J. S. Seroussi, History, mass loss, structure, and dynamic behavior of the Antarctic ice sheet. *Science* **367**, 1321–1325 (2020).
3. H. Gao, Analysis of new energy-saving technology for cold chain logistics. *IOP Conf. Ser. Earth Environ. Sci.* **252**, 032007 (2019).
4. *IIR-UN environment cold chain brief on cold storage and refrigerated warehouse* (UN-Environment-and-IIR, 2018); https://wedocs.unep.org/bitstream/handle/20.500.11822/32568/8138Warehouse_EN.pdf?sequence=1.
5. J. A. Evans, J.-M. Huet, L. Reinholdt, K. Fikiin, C. Zilio, M. Houska, C. Bond, M. Sheurs, T. W. M. Van Sambeek, Cold store energy usage and optimisation, in *Proceedings of the 23th International Congress of Refrigeration* (2011); https://researchgate.net/profile/Kostadin-Fikiin/publication/282135670_Cold_store_energy_usage_and_optimization/links/56049cce08aeb5718ff00d16/Cold-store-energy-usage-and-optimization.pdf.
6. W. Li, S. Fan, Radiative cooling: harvesting the coldness of the universe. *Opt. Photonics News* **30**, 32–39 (2019).
7. B. Zhao, M. K. Hu, X. Z. Ao, N. Chen, G. Pei, Radiative cooling: A review of fundamentals, materials, applications, and prospects. *Appl. Energy* **236**, 489–513 (2019).
8. M. Santamouris, J. Feng, Recent progress in daytime radiative cooling: Is it the air conditioner of the future. *Buildings* **8**, 168 (2018).
9. M. M. Hossain, M. Gu, Radiative cooling: principles, progress, and potentials. *Adv. Sci.* **3**, 1500360 (2016).
10. J. Mandal, Y. Yang, N. Yu, A. P. Raman, Paints as a scalable and effective radiative cooling technology for buildings. *Joule* **4**, 1350–1356 (2020).
11. J. N. Munday, Tackling climate change through radiative cooling. *Joule* **3**, 2057–2060 (2019).
12. P. Hsu, X. Li, Photon-engineered radiative cooling textiles. *Science* **370**, 784–785 (2020).
13. X. Lim, The super-cool materials that send heat to space. *Nature* **577**, 18–20 (2020).
14. A. R. Gentle, G. B. Smith, Radiative heat pumping from the earth using surface phonon resonant nanoparticles. *Nano Lett.* **10**, 373–379 (2010).
15. B. Bhatia, A. Leroy, Y. Shen, L. Zhao, M. Gianello, D. Li, T. Gu, J. Hu, M. Soljačić, E. N. Wang, Passive directional sub-ambient daytime radiative cooling. *Nat. Commun.* **9**, 5001 (2018).
16. X. Yin, R. Yang, G. Tan, S. Fan, Terrestrial radiative cooling: Using the cold universe as a renewable and sustainable energy source. *Science* **370**, 786–791 (2020).
17. A. P. Raman, M. A. Anoma, L. Zhu, E. Rephaeli, S. Fan, Passive radiative cooling below ambient air temperature under direct sunlight. *Nature* **515**, 540–544 (2014).
18. N. N. Shi, C. Tsai, F. Camino, G. D. Bernard, N. Yu, R. Wehner, Keeping cool: Enhanced optical reflection and radiative heat dissipation in Saharan silver ants. *Science* **349**, 298–301 (2015).
19. H. Zhang, K. C. S. Ly, X. Liu, Z. Chen, M. Yan, Z. Wu, X. Wang, Y. Zheng, H. Zhou, T. Fan, Biologically inspired flexible photonic films for efficient passive radiative cooling. *Proc. Natl. Acad. Sci.* **117**, 14657–14666 (2020).
20. P. Hsu, A. Y. Song, P. B. Catrysse, C. Liu, Y. Peng, J. Xie, S. Fan, Y. Cui, Radiative human body cooling by nanoporous polyethylene textile. *Science* **353**, 1019–1023 (2016).
21. J. Mandal, Y. Fu, A. C. Overvig, M. Jia, K. Sun, N. N. Shi, H. Zhou, X. Xiao, N. Yu, Y. Yang, Hierarchically porous polymer coatings for highly efficient passive daytime radiative cooling. *Science* **362**, 315–319 (2018).
22. Y. Zhai, Y. Ma, S. N. David, D. Zhao, R. Lou, G. Tan, R. Yang, X. Yin, Scalable-manufactured randomized glass-polymer hybrid metamaterial for daytime radiative cooling. *Science* **355**, 1062–1066 (2017).
23. L. Zhou, H. Song, J. Liang, M. Singer, M. Zhou, E. Stegenburgs, N. Zhang, C. Xu, T. Ng, Z. Yu, B. Ooi, Q. Gan, A polydimethylsiloxane-coated metal structure for all-day radiative cooling. *Nat. Sustain.* **2**, 718–724 (2019).
24. T. Li, Y. Zhai, S. He, W. Gan, Z. Wei, M. Heidarinejad, D. Dalgo, R. Mi, X. Zhao, J. Song, J. Dai, C. Chen, A. Aili, A. Vellore, A. Martini, R. Yang, J. Srebric, X. Yin, L. Hu, A radiative cooling structural material. *Science* **364**, 760–763 (2019).
25. X. Li, J. Peoples, P. Yao, X. Ruan, Ultrawhite BaSO4Paints and films for remarkable daytime subambient radiative cooling. *ACS Appl. Mater. Interfaces* **13**, 21733–21739 (2021).
26. S. H. Nile, V. Baskar, D. Selvaraj, A. Nile, J. Xiao, G. Kai, Nanotechnologies in food science: Applications, recent trends, and future perspectives. *Nano Micro Lett.* **12**, 45 (2020).
27. H. P. Huntington, Fragility and recovery in the Arctic. *Environ. Sci. Policy Sustain. Dev.* **60**, 26–29 (2018).
28. P. Convey, L. S. Peck, Antarctic environmental change and biological responses. *Sci. Adv.* **11**, eaaz0888 (2019).
29. N. Lucas, C. Bienaime, C. Belloy, M. Queneudec, F. Silvestre, J. Nava-Saucedo, Polymer biodegradation: Mechanisms and estimation techniques—A review. *Chemosphere* **73**, 429–442 (2008).
30. J. Puls, S. A. Wilson, D. Hölter, Degradation of cellulose acetate-based materials: A review. *J. Polym. Environ.* **19**, 152–165 (2011).
31. D. Hölter, P. Lapersonne, New Aspects of Cellulose Acetate Biodegradation (Cerdia, 2017); www.coresta.org/sites/default/files/abstracts/2017_ST13_Holter.pdf.
32. A. C. Albertsson, S. J. Huang, *Degradable Polymers, Recycling, and Plastics Waste Management* (Marcel Dekker Inc., 1995).
33. J. Yang, J. Li, Self-assembled cellulose materials for biomedicine: A review. *Carbohydr. Polym.* **181**, 264–274 (2018).
34. N. Hilal, A. F. Ismail, T. Matsuura, D. Oatley-Radcliffe, *Membrane Characterization* (Elsevier, 2017).
35. D. Li, X. Liu, W. Li, Z. Lin, B. Zhu, Z. Li, J. Li, B. Li, S. Fan, J. Xie, J. Zhu, Scalable and hierarchically designed polymer film as a selective thermal emitter for high-performance all-day radiative cooling. *Nat. Nanotechnol.* **16**, 153–158 (2021).
36. P. R. Griffiths, J. A. D. Haseth, J. D. Winefordner, *Fourier Transform Infrared Spectrometry* (John Wiley & Sons, 2007).
37. R. S. Bretzlaff, R. P. Wool, Frequency shifting and asymmetry in infrared bands of stressed polymers. *Macromolecules* **16**, 1907–1917 (1983).
38. H. Hagemann, R. G. Snyder, A. J. Peacock, L. Mandelkern, Quantitative infrared methods for the measurement of crystallinity and its temperature dependence: Polyethylene. *Macromolecules* **22**, 3600–3606 (1989).
39. J. Hendriksa, P. Pellikkaa, J. Peltoniemib, Estimation of anisotropic radiance from a glacier surface by comparing zenith measurements to satellite-derived albedos-preliminary results (2003); www.researchgate.net/publication/228399536_Estimation_of_anisotropic_radiance_from_a_glacier_surface_by_comparing_zenith_measurements_to_satellite_derived_albedos-Preliminary_results.
40. B. D. Mauro, G. Baccolo, R. Garzonio, C. Giardino, D. Massabò, A. Piazzalunga, M. Rossini, R. Colombo, Impact of impurities and cryoconite on the optical properties of the Morteratsch Glacier (Swiss Alps). *Cryosphere* **11**, 2393–2409 (2017).
41. X. Huang, X. Chen, M. Flanner, P. Yang, D. Feldman, C. Kuo, Improved representation of surface spectral emissivity in a global climate model and its impact on simulated climate. *J. Clim.* **31**, 3711–3727 (2018).
42. Rayleigh, The principle of similitude. *Nature* **95**, 66–68 (1915).
43. S. J. Hassol, *Impacts of a Warming Arctic: Arctic Climate Impact Assessment* (Cambridge Univ. Press, 2004).
44. A. Sorteberg, V. Kattsov, J. E. Walsh, T. Pavlova, The Arctic surface energy budget as simulated with the IPCC AR4 AOGCMs. *Clim. Dyn.* **29**, 131–156 (2007).
45. A. Senesea, R. S. Azzonia, D. Maragnoa, C. D'Agataa, D. Fugazzaa, B. Mosconia, A. Trentib, E. Meraldic, C. Smiragliaa, G. Diolaiutia, The non-woven geotextiles as strategies for mitigating the impacts of climate change on glaciers. *Cold Reg. Sci. Technol.* **173**, 103007 (2020).
46. Huaxia, "Chinese scientists cover glacier with blankets to slow melt," Xinhua Net, 5 January 2021; www.xinhuanet.com/english/2021-01/05/c_139643061.htm.
47. D. Zhao, A. Aili, Y. Zhai, S. Xu, G. Tan, X. Yin, R. Yang, Radiative sky cooling: Fundamental principles, materials, and applications. *Appl. Phys. Rev.* **6**, 021306 (2019).

48. A. C. Adolph, M. R. Albert, D. K. Hall, Near-surface temperature inversion during summer at Summit, Greenland, and its relation to MODIS-derived surface temperatures. *Cryosphere* **12**, 907–920 (2018).
49. A. Leroy, B. Bhatia, C. C. Kelsall, A. Castillejo-Cuberos, M. Di Capua, H. L. Zhao, L. Zhang, A. M. Guzman, E. N. Wang, High-performance subambient radiative cooling enabled by optically selective and thermally insulating polyethylene aerogel. *Sci. Adv.* **5**, eaat9480 (2019).
50. K. Krishnamurthy, H. K. Khurana, J. Soojin, J. Irudayaraj, A. Demirci, Infrared heating in food processing: An overview. *Compr. Rev. Food Sci. Food Saf.* **7**, 2–13 (2008).
51. S. A. Aboud, A. B. Altemimi, A. R. S. Al-Hilphy, L. Yi-Chen, F. Cacciola, A comprehensive review on infrared heating applications in food processing. *Molecules* **24**, 4125 (2019).
52. M. Kamruzzaman, Y. Makino, S. Oshita, Online monitoring of red meat color using hyperspectral imaging. *Meat Sci.* **116**, 110–117 (2016).
53. A. López-Maestresalas, K. Insausti, C. Jarén, C. Pérez-Roncal, O. Urrutia, M. J. Beriain, S. Arazuri, Detection of minced lamb and beef fraud using NIR spectroscopy. *Food Control* **98**, 465–473 (2019).
54. J. Nowatzki, R. Andres, K. Kyllo, Agricultural remote sensing basics (2004); http://hdl.handle.net/10365/5408.
55. M. Zeyghami, D. Y. Goswami, E. Stefanakos, A review of clear sky radiative cooling developments and applications in renewable power systems and passive building cooling. *Sol. Energy Mater. Sol. Cells* **178**, 115–128 (2018).
56. Y. Etzion, E. Erell, Thermal storage mass in radiative cooling systems. *Build. Environ.* **26**, 389–394 (1991).
57. C. F. Bohren, D. R. Huffman, *Absorption and Scattering of Light by Small Particles* (John Wiley & Sons, 2008).
58. S. Chandrasekhar, *Radiative Transfer* (Courier Corporation, 2013).
59. T. M. J. Nilsson, G. A. Niklasson, Radiative cooling during the day: Simulations and experiments on pigmented polyethylene cover foils. *Sol. Energy Mater. Sol. Cells* **37**, 93–118 (1995).
60. Q. Wang, P. Lu, M. Leppäranta, B. Cheng, G. Zhang, Z. Li, Physical properties of summer sea ice in the pacific sector of the Arctic during 2008–2018. *J. Geophys. Res.: Oceans* **125**, e2020JC016371 (2020).
61. A. Riihelä, T. Manninen, V. Laine, Observed changes in the albedo of the Arctic sea-ice zone for the period 1982–2009. *Nat. Clim. Chang.* **3**, 895–898 (2013).
62. A. Sorteberg, V. Kattsov, J. E. Walsh, T. Pavlova, Observed changes in the albedo of the Arctic sea-ice zone for the period 1982–2009. The Arctic surface energy budget as simulated with the IPCC AR4 AOGCMs. *Clim. Dyn.* **29**, 131–156 (2007).
63. H. Hersbach, B. Bell, P. Berrisford, S. Hirahara, A. Horányi, J. Munoz-Muñoz-Sabater, J. Nicolas, C. Peubey, R. Radu, D. Schepers, A. Simmons, C. Soci, S. Abdalla, X. Abellan, G. Balsamo, P. Bechtold, G. Biavati, J. Bidlot, M. Bonavita, G. D. Chiara, P. Dahlgren, D. Dee, M. Diamantakis, R. Dragani, J. Flemming, R. Forbes, M. Fuentes, A. Geer, L. Haimberger, S. Healy, R. J. Hogan, E. Hólm, M. Janisková, S. Keeley, P. Laloyaux, P. Lopez, C. Lupu, G. Radnoti, P. D. Rosnay, I. Rozum, F. Vamborg, S. Villaume, J. Thépaut, The ERA5 global reanalysis. *Q. J. R. Meteorol. Soc.* **146**, 1999–2049 (2020).
64. S. Dobricic, L. Pozzoli, *Arctic Permafrost Thawing* (Publications Office of the European Union, 2019).
65. G. Danabasoglu, J.-F. Lamarque, J. Bacmeister, D. A. Bailey, A. K. DuVivier, J. Edwards, L. K. Emmons, J. Fasullo, R. Garcia, A. Gettelman, C. Hannay, M. M. Holland, W. G. Large, P. H. Lauritzen, D. M. Lawrence, J. T. M. Lenaerts, K. Lindsay, W. H. Lipscomb, M. J. Mills, R. Neale, K. W. Oleson, B. Otto-Bliesner, A. S. Phillips, W. Sacks, S. Tilmes, L. van Kampenhout, M. Vertenstein, A. Bertini, J. Dennis, C. Deser, C. Fischer, B. Fox-Kemper, J. E. Kay, D. Kinnison, P. J. Kushner, V. E. Larson, M. C. Long, S. Mickelson, J. K. Moore, E. Nienhouse, L. Polvani, P. J. Rasch, W. G. Strand, The Community Earth System Model version 2 (CESM2). *J. Adv. Model. Earth Syst.* **12**, e2019MS001916 (2020).
66. E. Hunke, W. Lipscomb, A. Turner, N. Jeffery, S. Elliot, *The Los Alamos Sea Ice Model. Documentation and Software User's Manual. Version 5.1* (Los Alamos National Laboratory, 2015).
67. P. Briegleb, B. Light, *A Delta-Eddington Mutiple Scattering Parameterization for Solar Radiation in the Sea Ice Component of the Community Climate System Model* (University Corporation-for-Atmospheric-Research, 2007); https://opensky.ucar.edu/islandora/object/technotes:484.
68. L. Field, D. Ivanova, S. Bhattacharyya, V. Mlaker, A. Sholtz, R. Decca, A. Manzara, D. Johnson, E. Christodoulou, P. Walter, K. Katuri, Increasing Arctic sea ice albedo using localized reversible geoengineering. *Earth's Future* **6**, 882–901 (2018).
69. Y. H. Chen, X. L. Huang, X. H. Chen, M. Flanner, The effects of surface longwave spectral emissivity on atmospheric circulation and convection over the Sahara and Sahel. *J. Clim.* **32**, 4873–4890 (2019).
70. B. E. J. Rose, CLIMLAB: A Python toolkit for interactive, process-oriented climate modeling. *J. Open Source Softw.* **3**, 659 (2018).

Acknowledgments: We acknowledge the microfabrication center of the National Laboratory of Solid State Microstructures (NLSSM) for technique support. J.Z. acknowledges the support from the XPLORER PRIZE. Y.L. and M.W. acknowledge the High Performance Computing Center of Nanjing University and the Beijing Paratera Technology Co. Ltd. for the help with the climate simulation. **Funding:** This work is jointly supported by the National Key Research and Development Program of China (nos. 2021YFA140070 and 2017YFA0205700), National Natural Science Foundation of China (nos. 52102262, 52002168, 12022403, 51925204, 11874211, and 61735008), Natural Science Foundation of Jiangsu Province (nos. BK20200340 and BK20190311), Excellent Research Program of Nanjing University (ZYJH005), research foundation of Frontiers Science Center for Critical Earth Material Cycling (JBGS2106), and the Fundamental Research Funds for the Central Universities (nos. 021314380184, 021314380208, 021314380190, 021314380140, and 021314380150). M.W. is supported by the Natural Science Foundation of China (nos. 41925023, 91744208, 41575073, and 41621005), the Minister of Science and Technology of China (nos. 2017YFA0604002 and 2016YFC0200503), and the Collaborative Innovation Center of Climate Change, Jiangsu Province. W.L. and S.F. acknowledge funding support from the U.S. Department of Energy under grant no. DE-FG02-07ER46426. Z.W. acknowledges funding support from the National Natural Science Foundation of China (no. 21805132). **Author contributions:** J.Z., M.W., J.L., and N.X. conceived and planned this research. J.L., N.X., B.Z., Z.W., and X.W. performed the experiments. Y.L. and M.W. contributed to the climate modeling. J.L. and W.L. performed the thermal analysis. J.L., Y.L., W.L., N.X., S.F., M.W., B.Z., and J.Z. organized the data and wrote the manuscript. All authors discussed the results and approved the final version of the manuscript. **Competing interests:** The authors declare that they have no competing interests. **Data and materials availability:** All data needed to evaluate the conclusions in the paper are present in the paper and/or the Supplementary Materials.

Submitted 16 June 2021
Accepted 20 December 2021
Published 11 February 2022
10.1126/sciadv.abj9756

ScienceAdvances

Protecting ice from melting under sunlight via radiative cooling

Jinlei LiYuan LiangWei LiNing XuBin ZhuZhen WuXueyang WangShanhui FanMinghuai WangJia Zhu

Sci. Adv., 8 (6), eabj9756. • DOI: 10.1126/sciadv.abj9756

Science Advances (ISSN) is published by the American Association for the Advancement of Science. 1200 New York Avenue NW, Washington, DC 20005. The title *Science Advances* is a registered trademark of AAAS.